11th International Workshop on Ship and Marine Hydrodynamics
Hamburg, Germany, September 22-25, 2019

Experimental and Numerical Evaluation of the Added Wave Resistance for an Ultra Large Container Ship in Shallow Water

Luca Donatini[1,*], Manasés Tello Ruiz[1,*], Guillaume Delefortrie[1,2], José C. Villagómez[2], Marc Vantorre[1] , Evert Lataire[1]

[1]Ghent University, Maritime Technology Division
Technologiepark 60, 9052 Ghent, Belgium

[2]Flanders Hydraulics Research
Berchemlei 115, 2140 Antwerp, Belgium

*Corresponding authors, luca.donatini@ugent.be, manases.ruiz@ugent.be

ABSTRACT

In this paper, the added wave resistance of an Ultra Large Container Ship (ULCS) in shallow water is investigated both experimentally and numerically. The experimental results come from a series of tests performed in the Towing Tank for Manoeuvres in Confined Water (co-operation Flanders Hydraulics Research and Ghent University) in Antwerp (Belgium) in 2016. Tests were executed for head and following waves, with two wave amplitudes, and using two different beam frames to attach the ship to the towing tank's carriage. One of the frames restrained the heave and pitch motions while the other one allowed the free motion of both. The results of experiments outline the proportionality of added resistance on the square of the wave amplitude in shallow water conditions. Moreover, the expected behaviour of added resistance at different wave lengths can be observed: in long waves, the added resistance is tightly related to the ship motions, while in short waves it achieves an asymptotic trend. In following waves, a peculiar phenomenon is noticed: at moderate forward speeds a positive added resistance of substantial magnitude is measured for a specific, speed dependent interval of wave lengths. This phenomenon is investigated and preliminary ascribed to the interaction between the incident wave field and the return current originated by the motion of the ship in shallow water. Numerical simulations are performed with two potential codes: one based on strip theory and one 3D panel code. The 3D panel code performs better than the strip theory code. An in-depth analysis of the added resistance and vertical motions is performed, and the discrepancies of simulated added resistance with respect to experiments are mainly ascribed to the inaccuracies of numerical codes in the calculation of heave and pitch RAOs and phases.

1 INTRODUCTION

Container ship traffic has flourished over the last decades, accompanied by a constant increase in the main dimensions of container vessels, which now fall under the category of Ultra Large Container Ships (ULCS). Concurrently to the growth in size of container ships, the increase in fuel prices and the tightening of emission standards stimulated studies to reduce fuel consumption by optimizing the ship resistance and propulsion. Since the influence of waves can increase significantly the power required to attain a certain ship speed, and therefore the fuel consumption, added resistance in waves has received a major attention in literature, where it has been studied by means of both experiments and numerical simulations. Often, the added resistance has been simulated starting from the solution of the seakeeping problem provided by potential flow solvers in the frequency domain. To this end, two main analytical methods have been presented and widely used in literature: the so called far-field and near-field methods. The far field method is based on the conservation of momentum in the fluid surrounding the ship. The momentum generated by the ship is evaluated across a control surface far from the ship and considered equal to the mean force acting on the ship. This approach was

introduced by Maruo [1] and further extended by Joosen [2] and Newman [3]. A simplified method, based on the radiated wave energy, was proposed later in [4]. More recently, the far-field approach was applied in [5], using frequency domain and more advanced time domain potential codes for the solution of the seakeeping problem.

The near-field method, on the other hand, is based on a direct integration of the hydrodynamic pressure acting on the wetted surface of the hull. This method was introduced by Havelock [6], who only considered the pressure induced by the incident wave according to the Froude-Krylov approach. The near-field method was extended by Boese [7], who proposed a more advanced formulation based on the full Bernoulli equation, but did not include all terms. Later on, Pinkster [8] and Faltinsen et al. [9] proposed a 3D formulation which is exact to the second order for the zero-speed and forward speed cases, respectively.

The near-field method gained popularity also because of its more intuitive nature, which makes it easier to understand the physics behind added resistance [10]. In [8], Pinkster breaks up the full formulation for the wave added resistance based on the integration of the second order pressure into five components, attributed to: (a) the first order relative wave elevation along the waterline; (b) the pressure drop due to first order velocity; (c) the pressure due to the product of gradient of first order pressure and first order motions; (d) the contribution due to products of first order angular motions and inertia forces; and finally (e) the contribution of second order potential. The last term (e), due to the second order potential, vanishes in regular waves.

Among the first four terms present in regular waves, the first term due to the relative wave elevation is described to be dominant [8]. The effects of this term on the total added resistance are only marginally reduced by the other three terms (b), (c) and (d). Therefore, the total added resistance plotted against the wave length is expected to mirror the trend outlined by the first term alone, with a reduced magnitude due to the reducing effects of the other terms as shown in [11]. In head and following waves, when roll motion is supposed to be absent, the relative wave elevation along the waterline depends on the combined effects of the first order wave profile and of the first order pitch and heave motions. Both the amplitudes and phases of these three elements play a role. In head and following waves the Response Amplitude Operators (RAO) and phases of the heave and pitch motions are crucial for a correct determination of the total added resistance in waves, as confirmed also in several other works like [5], [10], [12], [13] and [14] among others.

Both the far-field and the near-field methods have proven to be sufficiently accurate in the long wave length range (waves longer than about half of the ship's length) where the added resistance is dominated by the effects of ship motions. In short waves, however, the physical phenomenon at the origin of added resistance changes: in this range of wave lengths the ship motions are very small and incoming waves are mostly reflected by the ship hull which acts like a wall. Due to this, the added resistance reaches an asymptotic behaviour. A first semi-empirical formulation to calculate the added resistance in short waves, based on the assumption that the ship behaves like a vertical wall of limited draft, was derived by Fujii and Takahashi [15] and further expanded by Faltinsen et al. [9]. More recently, corrections to the previous formulations were introduced in [16] and [17] to take into account more modern ship forms, focussing on the effects of the flare angle of the sides, especially relevant for finer hull forms, and of transom sterns. Due to the large dimensions of modern ULCS, most of the wave conditions encountered in coastal areas or in confined seas would be suited for the application of short waves formulations [16]. This is especially true in shallow water conditions, where the occurring wave lengths are physically limited.

Recently, thanks to the increase in power of computational facilities, the problem of added resistance has also been studied by means of Computational Fluid Dynamics (CFD) simulations. Even if it is generally accepted that the added resistance is mainly due to pressure effects, while frictional effects are negligible, CFD simulations have some advantages over the potential flow approach despite the much heavier computational requirements. These codes provide the added resistance as a direct result, without the need of additional theories, like the far-field or near-field methods required to process the results of potential codes. Another advantage is the possibility to take into account viscous effects impacting, albeit marginally, the vertical motions. The vertical motions of heave and pitch are usually slightly overestimated by potential codes near the resonance frequency due to a lack of damping [18], and this effect is reflected in the added resistance. Finally, CFD calculations allow to account for steeper waves [19] and heavily non-linear flow phenomena, such as green water on deck and breaking waves [12].

Research on the topic of added resistance in waves has been mostly focused on deep water conditions, while the wave added resistance in shallow water has been addressed by few. In [20], the behaviour of the KVLCC2 vessel in regular waves was investigated for different Under Keel Clearances (UKC) and ship speeds, in terms of both motions and mean drift forces. In [21] and [22], the results of experimental tests on an ULCS are presented for the first time. Recently, Martić et al. [23] investigated the added resistance of the DTC

container vessel in head waves, for two under keel clearances (UKCs) and two forward speeds, by a comparison of CFD calculations with the results of tests performed within the framework of the SHOPERA project [24]. The conclusions of [23] outline a satisfactory agreement between the numerical and experimental results, and confirm the dominant role of pressure effects on the development of added resistance.

The present work investigates the added resistance of an ULCS in both head and following waves, in shallow water conditions identified by a non-dimensional UKC (see definition in 2.1.3) of 50%. The study investigates in detail the experimental results partially presented in [21] and [22] and compares them with the numerical results produced by two potential codes. The paper is organized as follows: Chapter 2 describes the methodology followed in both the experimental campaign and numerical simulations; Chapter 3 presents the results obtained from experiments and simulations for added resistance and vertical motions (heave and pitch); Chapter 4 discusses three interesting aspects which were outlined by the results and finally Chapter 5 draws the conclusions laying the ground for future research on the topic.

2 METHODOLOGY

2.1 Experimental study

The experimental results presented here come from a series of tests performed in the Towing Tank for Manoeuvres in Confined Water (co-operation Flanders Hydraulics Research and Ghent University) in Antwerp (Belgium) in 2016 to investigate the manoeuvring behaviour in shallow water of an ULCS.

2.1.1 Towing tank and wave gauges

The Towing Tank for Manoeuvres in Confined Water is owned, maintained and operated by Flanders Hydraulics Research in co-operation with Ghent University, and has the following main dimensions: a useful length of 68.0 m, a width of 7.0 m and a maximum water depth of 0.5 m. The towing tank is equipped with a carriage mechanism which allows to perform both captive and free running tests. The ship model can be connected to the main carriage through two different beam frames, A and B, which allow semi-captive and fully captive tests respectively. In semi-captive tests, the roll and pitch motions of the ship model are allowed by roll and pitch mechanisms while the heave motion is allowed by a vertical guidance system. Beam frame A is fitted with two load cells, measuring transverse and longitudinal forces, and four potentiometers measuring vertical motions. In fully captive tests with frame B, the roll, pitch and heave motions are restricted by the frame, and six strain gauges are used to calculate forces and moments in 6 DOF.

The presence of a piston-type wave generator at the end of the towing tank allows to generate both regular and irregular long crested waves. In order to record waves during tests, five wave gauges are installed in the towing tank: four of them (WG1 to WG4) are of the resistant type and placed at fixed locations on the right side of the tank, while one (WG6) is a laser beam gauge, attached to the carriage in front of the ship and moving with it during the test. The main parameters of the towing tank and the position of wave gauges are shown in Figure 1. For additional, more detailed information concerning the Towing Tank for Manoeuvres in Confined Water, the reader is referred to [25].

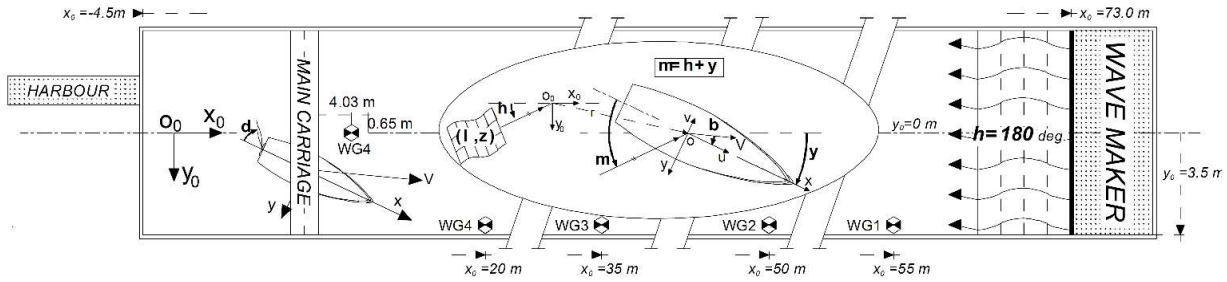

Figure 1: Towing tank parameters and wave gauges position. Retrieved from [22].

2.1.2 Ship model

The test campaign was performed with a scale model ($\lambda = 90$) of an Ultra Large Container Ship, referred to as *C0W*. The main characteristics of the ship under investigation are presented in Table 1.

Table 1: Main particulars of the ULCS *C0W* at model and full scale.

Item	Model scale		Full scale	
	Value	Units	Value	Units
L_{OA}	4418	[mm]	397.6	[m]
L_{PP}	4191	[mm]	377.2	[m]
B	627	[mm]	56.4	[m]
D	330	[mm]	29.7	[m]
T_{M}	145.6	[mm]	13.1	[m]
C_{B}	0.6	[-]	0.6	[-]
m	226.4	[kg]	165046	[ton]
k_{xx}	212	[mm]	19.1	[m]
k_{yy}	1029	[mm]	92.6	[m]
k_{zz}	1054	[mm]	94.9	[m]
X_{CG}	-108	[mm]	-9.7	[m]
Y_{CG}	0	[mm]	0	[m]
Z_{CG}	0	[mm]	0	[m]

2.1.3 Tests setup, ship speeds and water depth

Among the large amount of tests performed in the framework of the experimental campaign of 2016 only steady straight line tests where the ship is towed by the carriage (captive configuration) are analysed in this paper. Both the results obtained from beam frame A and beam frame B (see 2.1.1) are considered.

Five different ship speeds were tested, as summarized in Table 2. For tests with beam frame B the last speed, corresponding to 15 knots at full scale, was not tested due to the fact that the expected large squat effects would be prevented by the fully captive frame, leading to an unrealistic condition.

Table 2: Ship speeds at full and model scale.

Speed ID	Fr [-]	V_{ship} [kn]	V_{model} [m/s]
S1	0.025	3.0	0.163
S2	0.050	6.0	0.325
S3	0.075	9.0	0.488
S4	0.100	12.0	0.651
S5	0.125	15.0	0.813

The test campaign included tests performed with two non-dimensional UKC values (50% and 35%). The non-dimensional UKC is defined here as the ratio between the UKC and the draft of the vessel. In this paper, only tests with a non-dimensional UKC of 50%, corresponding to a water depth of 218 mm at model scale and of 19.6 m at full scale, are analysed in order to exclude larger squat effects corresponding to the lower UKC value. These effects could again lead to unrealistic conditions when using beam frame B.

2.1.4 Wave characteristics

Steady straight line tests were performed in calm water as well as in waves, allowing to calculate the added resistance induced by regular waves. The tests were performed with both head (μ = 180 deg) and following waves (μ = 0 deg), where the latter condition was obtained by rotating the ship model and by making the carriage run in the opposite direction i.e. from the wave maker towards the harbour (see Figure 1).

Tests were performed with a wave amplitude ζ_{A} = 11.1 mm, corresponding to ζ_{A} = 1.0 m at full scale. Additional tests were performed with a wave amplitude ζ_{A} = 15.0 mm (1.35 m at full scale) to investigate the

dependency of the wave added resistance in shallow water on the wave amplitude. These tests were only performed for head waves and for speeds S1, S3 and S5.

Nine different wave frequencies (w1 to w9) were tested in the experiments, corresponding to wave lengths ranging from 0.2 and 0.8 times the ship's length (L_{PP}). The main characteristics of the selected regular waves are shown in Table 3. The wave lengths are calculated based on a water depth of 218 mm at model scale and of 19.6 m at full scale. The last wave frequency, w9, was only tested with the smaller wave amplitude of 11.1 mm. The same regular waves were tested in both head and following configurations.

Table 3: Main wave characteristics: wave length λ_W, wave angular frequency ω and wave amplitude ζ_A.

Item	L_{PP}/λ_W [-]	Model scale		Full scale		ζ_A [mm]
		λ_W [m]	ω[rad/s]	λ_W [m]	ω [rad/s]	
w1	5.00	0.84	8.26	75.4	0.87	11.1; 15.0
w2	3.85	1.09	6.94	98.0	0.73	11.1; 15.0
w3	3.13	1.34	5.95	120.5	0.63	11.1; 15.0
w4	2.63	1.59	5.19	143.4	0.55	11.1; 15.0
w5	2.27	1.85	4.59	166.2	0.48	11.1; 15.0
w6	2.00	2.10	4.11	188.6	0.43	11.1; 15.0
w7	1.67	2.51	3.49	225.9	0.37	11.1; 15.0
w8	1.43	2.93	3.03	263.8	0.32	11.1; 15.0
w9	1.25	3.35	2.67	301.8	0.28	11.1

2.1.5 Post-processing

The output of the model test campaign have the form of time-series of physical quantities recorded by the wave gauges and by the potentiometers, strain gauges and load cells on the ship model. These time-series have to be post-processed in order to obtain frequency dependent values for the mean total forces acting on the vessel as well as RAOs of oscillatory motions. First of all, a limited time window is selected to isolate results where the incident wave field is regular and not contaminated by reflected waves and where the ship speed is stationary. Then, the signal is filtered in order to remove noise. This is done in two stages: first by using a low pass filter to remove all the high frequency noise, and then applying two band pass filters to isolate frequencies around the main frequency ω_1 and around a frequency equal to two times ω_1. Finally, a Fourier analysis of the selected and filtered data was performed by using a least square fit method to calculate the eight unknown parameters $(a_0, a_1, b_1, a_2, b_2, a_3, b_3, \omega_1)$ of a third order Fourier series:

$$f = a_0 + \sum_{j=1}^{3} a_j \cos(j\omega_1 t) + b_j \sin(j\omega_1 t) \quad (1)$$

The post-processing procedure was described in more detail in [26], [27] and more recently in [22]. The experimental value for added resistance in waves is obtained as the difference between the mean value (a_0) of the surge force obtained by post processing the results of experimental tests in waves and the total resistance R_T measured in calm water tests. The added resistance is presented in this paper by means of the non-dimensional coefficient defined as:

$$C_{AW} = R_{AW}/\left(\rho g \zeta_A^2 B^2 / L_{PP}\right) \quad (2)$$

2.1.6 Uncertainty

A preliminary uncertainty analysis concerning the accuracy of measured forces and moments was performed for frame B and speeds S2 and S3. The complete results of the uncertainty analysis are presented in [22]. A maximum uncertainty of around 4% was observed for surge forces and roll moments at the lower speed. For a higher speed, the uncertainty was found to be less.

2.2 Numerical simulations

A numerical investigation of the added resistance in shallow water of the ULCS *C0W* is carried out with the aim to evaluate the accuracy of added resistance prediction by potential codes in shallow water conditions.

The strip theory code Octopus Seaway and the 3D panel code Hydrostar are used for this purpose. For both codes, several different options to calculate the wave added resistance are tested in order to outline the ones providing the most accurate results in shallow water conditions. All the simulations were performed at real scale and in shallow but otherwise unrestricted water.

2.2.1 Hydrostar setup

Version 7.03 of the 3D panel code Hydrostar, developed by Bureau Veritas, was used to produce the results shown in this paper. Hydrostar is a linear 3D solver for the radiation/diffraction problem in the frequency domain, based on potential theory and Green Functions.

The hull of the *C0W* ULCS was meshed starting from 45 2D cross sections by means of the automatic mesh generation tool *AMG* part of the Hydrostar suite. The final mesh used for the simulations was made up of 982 quadrilateral panels, selected after a mesh independence study. Simulations were performed for an array of 50 regular waves, characterized by angular frequencies ranging from 0.02 rad/s up to 1.00 rad/s with an interval of 0.02 rad/s. Head and following waves were simulated by setting two values for the wave encounter direction, respectively of $\mu = 180$ deg and $\mu = 0$ deg.

Concerning the added resistance in waves, the near-field method was selected after preliminary simulations due to the inaccuracy shown by the other two available methods (far- and middle-field) when simulating cases with forward speed in shallow water. All the five speeds considered in the experimental campaign (see Table 2) were simulated, together with a zero speed case. The forward speed effects were accounted for through the default method, the encounter frequency approach, implemented in Hydrostar. The wave-current interaction approach, made available to the authors by Bureau Veritas with of a beta release of Hydrostar, was tested but not used in this paper due to its limitation to infinite depth cases.

2.2.2 Octopus Seaway setup

The strip theory code Octopus Office by ABB (version 6.4.14), and more specifically the Seaway module originally developed by Journée [28], was used. Due to the shallow water conditions, the *Keil*'s method for the calculation of 2D hydrodynamic coefficients was selected as suggested by [29]. Preliminary simulations confirmed the poor performances of other methods (e.g. *CloseFit* or *Frank*) in such shallow water conditions.

Concerning the calculation of wave loads, the option *diffraction wave loads* was preferred since it was found to substantially outperform the *classical wave loads* option, in agreement with the results in [30]. Concerning the type of strip theory formulation used, differences between the two possible options were much lower and finally the *modified strip theory* option, developed to account better for forward speed effects [28] was preferred to the *ordinary strip theory* option.

The ship speeds, wave frequencies and wave directions simulated with Seaway are the same as described in the previous section for Hydrostar. Concerning the calculation of added resistance, the pressure integration method (near field) implemented in Seaway was used rather than the far field method in order to compare the results with the ones from Hydrostar.

3 RESULTS

The results obtained from experimental tests and numerical simulations for oscillatory motions (heave and pitch) and for mean values of the added resistance in waves are shown here. An extensive discussion of the results is carried out in the next section. The phases of the motions are not included due to space limitations. Figure 2 and Figure 3 present the RAOs of pitch motion in head and following waves respectively. Figure 4 and Figure 5 present the RAOs for heave motion and finally Figure 6 and Figure 7 present the values of the mean added resistance in waves.

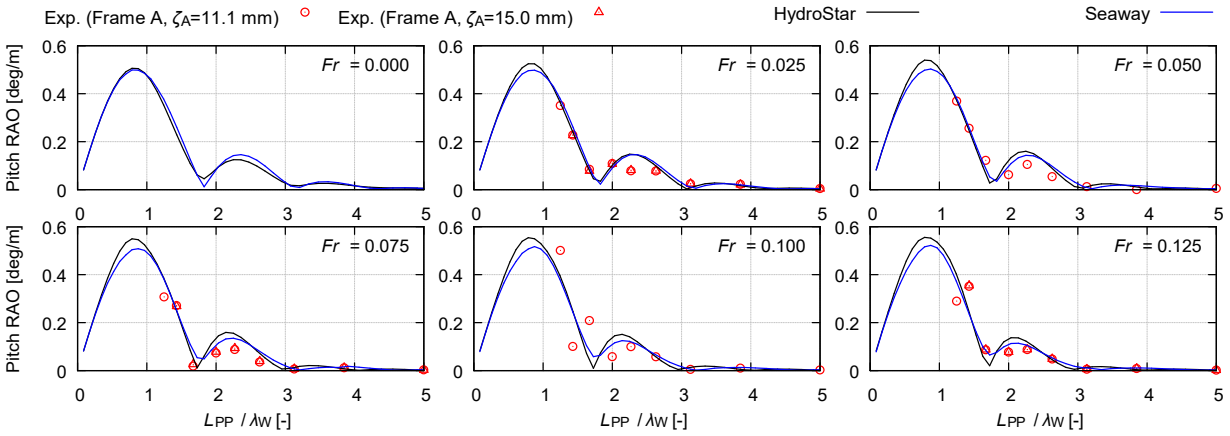

Figure 2: Pitch motion in head waves.

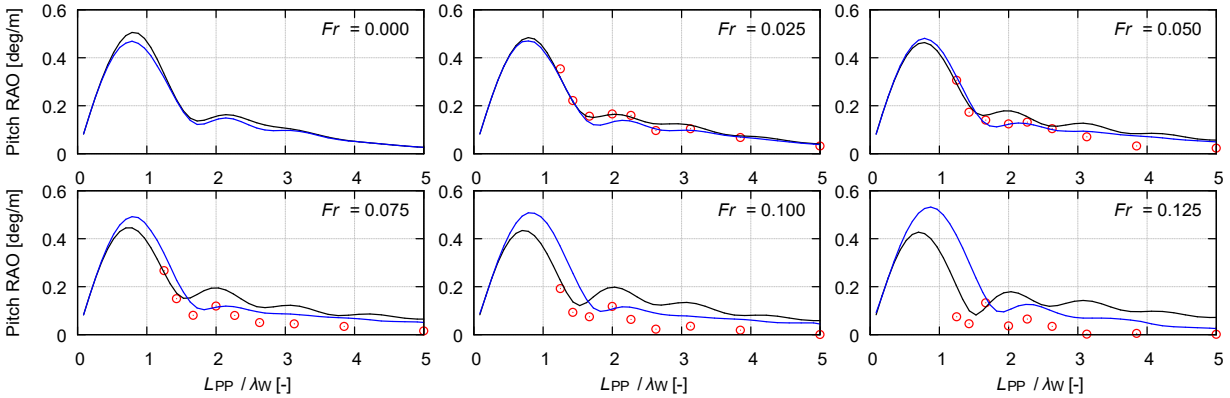

Figure 3: Pitch motion in following waves. Legend is the same as in Figure 2.

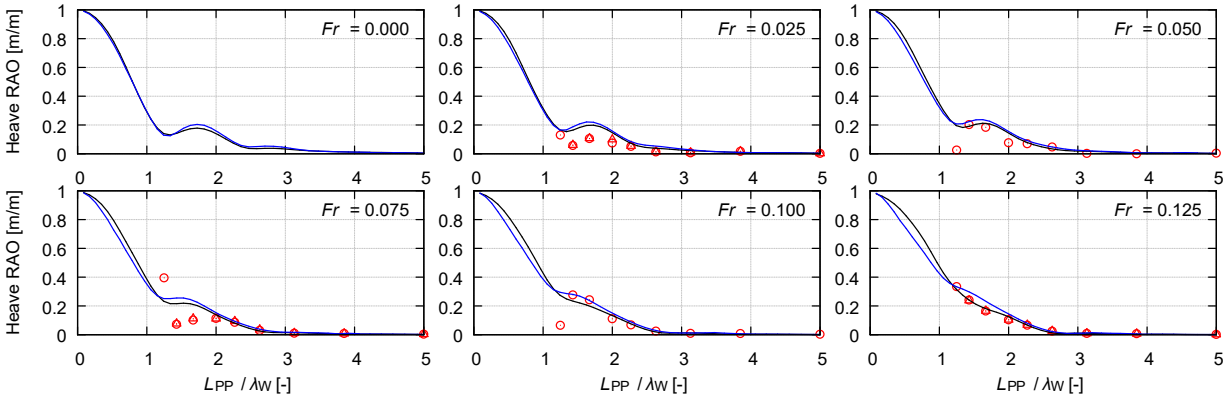

Figure 4: Heave motion in head waves. Legend is the same as in Figure 2.

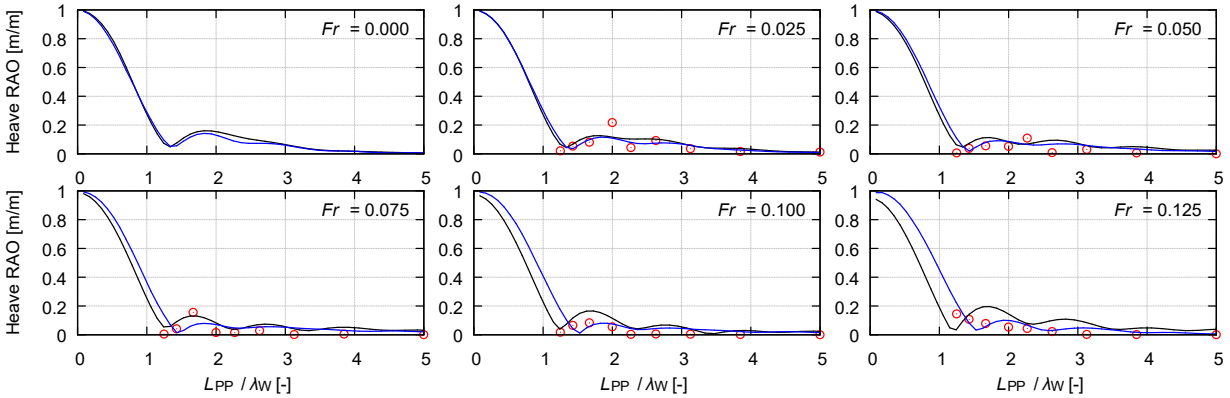

Figure 5: Heave motion in following waves. Legend is the same as in Figure 2.

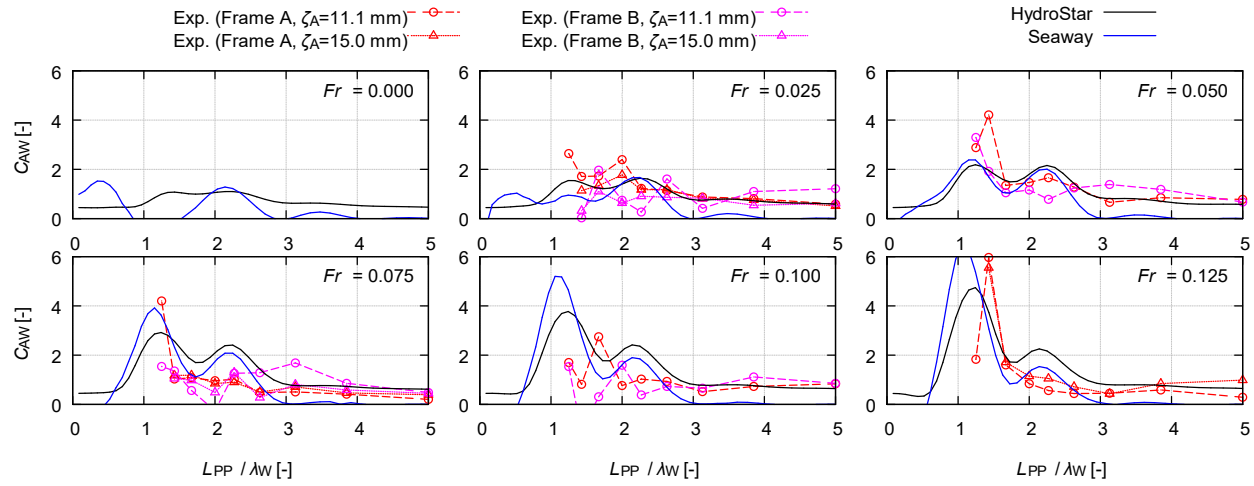

Figure 6: Added resistance in head waves.

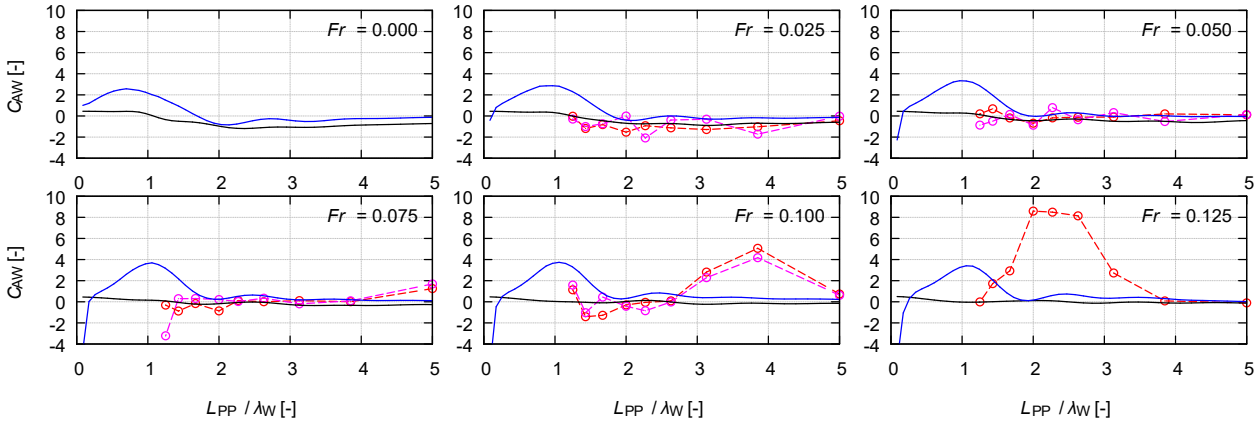

Figure 7: Added resistance in following waves. Legend is the same as in Figure 6.

4 DISCUSSION

4.1 Influence of motions and wave amplitude

The influence of ship motions and of the wave amplitude on the added resistance is investigated by means of an analysis of the experimental results. Concerning the influence of the wave amplitude on added resistance in shallow water, the linear dependence on the square of the wave amplitude, expected in deep water cases [18], is observed. This can be deduced from the results presented in Figure 6, where the curves of dimensionless measured data relative to the two wave amplitudes used in the tests show good agreement. For the semi-captive beam frame A, the agreement is very good. For the fully captive beam frame B, only speeds S1 and S3 (Fr = 0.025 and 0.075 respectively) were tested with both amplitudes. In this case, the agreement is slightly less good than the one found with beam frame A. At both speeds (Figure 6, top centre and bottom left), the added resistance measured with the smallest wave amplitude (magenta circles) shows an oscillating behaviour, which is not seen with the larger wave amplitude (magenta triangles). This is probably because the wave loads induced by the smallest amplitude waves are small enough to fall in the range of uncertainty of the measuring instruments fitted on beam frame B.

Concerning the influence of motions on the added resistance, the comparison between the experimental results obtained with frame A and the ones obtained with frame B predictably outlines some differences, especially in the wave length range corresponding to higher oscillatory motion responses (L_{PP}/λ_W = 1 to 3). This confirms the tight relationship between the ship motions and the added resistance in the long waves range pointed out in the introduction. In head waves, the expected asymptotic behavior of the added resistance due to the reflection of waves on the ship hull is observed in the low wave lengths range (L_{PP}/λ_W = 3 to 5). In this wave length range, a good agreement between all the experimental results (both beam frames and both wave amplitudes) can be observed.

4.2 Added resistance in following waves

An interesting phenomenon was noticed in the experimental results in following waves: for moderate speeds corresponding to Froude numbers above 0.075, a positive added resistance of important magnitude, higher than the one observed in head waves, appears in correspondence to a specific range of wave lengths. The magnitude of the maximum positive added resistance increases with the ship's forward speed, as do the wave lengths where the phenomenon starts to appear and where the phenomenon decays (lower L_{PP}/λ_W ratios). This can be clearly seen in Figure 7: for Fr = 0.075, a sudden increase of the added resistance can be seen between L_{PP}/λ_W ratios of 4 and 5; for Fr = 0.100, the added resistance increases around an L_{PP}/λ_W ratio of 2.6 and decreases back to zero at L_{PP}/λ_W = 5; finally, for Fr = 0.125, a full bell-shaped area of positive added resistance can be seen observed between L_{PP}/λ_W ratios of 1.2 and 4.

This peculiar phenomenon is hypothetically attributed to the interaction between the return current generated by the forward motion of the ship in shallow water and the incoming waves. In the case of following waves, the return current generated by the forward motion of the vessel acts as an opposing current. An opposing current introduces a Doppler effect on the dispersion relation and reduces the wave's length and the wave's phase and group velocity [31]. Waves propagate in an undisturbed field according to their group speed rather than their phase speed [32]. When the opposing current speed is equal to the waves group speed, a singularity point is reached where incoming waves cannot propagate further upstream [31]. In less extreme cases, an opposing current will slow down the group velocity and therefore the propagation of the disturbance.

In order to investigate the effect and verify the initial hypothesis, a preliminary calculation of the mean return flow on the midship section V_{ret} is performed according to Bernoulli and continuity equations, taking into consideration the size of the tank as well as the blockage induced by the ship and the experimentally measured water level decrease due to squat. A relative group velocity c_{GR} is calculated for each of the considered regular waves by subtracting the ship speed from the absolute group velocity c_{GA}. The results for the two highest ship speeds are summarized in Table 4.

Table 4: Group velocity of regular waves in opposing current with respect to the ship (model scale).

Fr	V_{ret}	Group velocity relative to ship c_{GR} [m/s]								
[-]	[m/s]	w9	w8	w7	w6	w5	w4	w3	w2	w1
0.100	0.070	0.700	0.668	0.624	0.557	0.500	0.425	0.326	0.196	0.036
0.125	0.090	0.537	0.506	0.461	0.394	0.338	0.263	0.163	0.033	-0.126

From this analysis, it appears clear that the interval of positive added resistance ends when the return flow V_{ret} is faster than the group velocity of waves relative to the ship c_{GR}. This occurs for the two shorter waves w1 and w2 at the higher speed (Fr = 0.125) and for wave w1 at the speed corresponding to Fr = 0.100. These three cases are shaded in Table 4. For longer waves, the wave disturbance can reach ship, but due to the return current the group velocity relative to the ship is low. Therefore, for a significant part of the test the ship lays between undisturbed flow at the bow and flow disturbed by waves at the stern, with the front of the disturbance slowly moving forward. The origin of the observed positive added resistance is ascribed to this peculiar flow condition, while a complete physical explanation of the phenomenon will require further research with more advanced tools like CFD simulations and ad-hoc designed experiments with advanced techniques for flow tracing and wave field identification.

The considerations above are confirmed by an analysis of the measurements of wave gauge WG3 (for the gauge position see Figure 1). The signals recorded by the wave gauge are disturbed by the close proximity of the tank wall, but they still outline an interesting pattern. In Figure 8, an example of WG3 recordings corresponding to the three meaningful cases is shown. In the plots, the theoretical time when the wave disturbance is expected to reach the wave gauge, according to the group velocity, is reported (red dashed line), together with the time window between the passage of the bow and of the stern of the ship at the longitudinal position of the wave gauge (blue dashed lines).

The wave gauge recordings show that for wave lengths lower than the one at which the added resistance starts to increase, waves are able to propagate over the ship so that the wave gauge records wave induced oscillations of the free surface well before the passage of the ship (e.g. Figure 8, bottom). For wave lengths corresponding to the positive added resistance range, a noticeable increase in the wave amplitude is observed during the passage of the ship at the wave gauge position, meaning that the wave disturbance builds up along the length of the ship (e.g. Figure 8, middle). Finally, for wave lengths where the positive added resistance

decays to zero, waves are only recorded after the passage of the ship, even if according to their group velocity they should already be recorded before the ship's passage (e.g. Figure 8, top). In these cases, the return flow is strong enough to keep the wave field behind the ship.

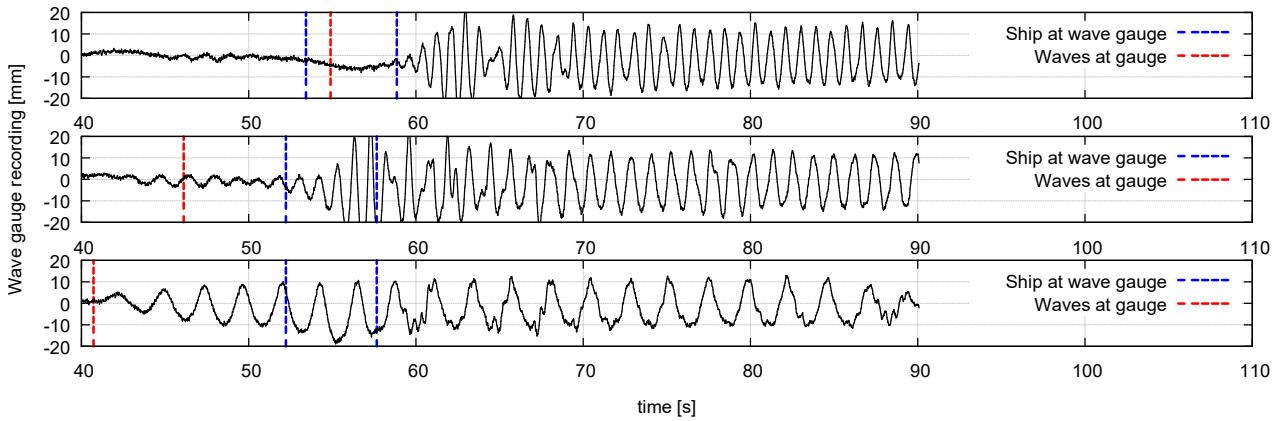

Figure 8: Recordings of wave gauge WG3 (Frame A, ζ_A = 11.1 mm, Fr = 0.125) for three regular waves: w2 (top), w4 (middle), w9 (bottom).

4.3 Accuracy of numerical models

The analysis of the accuracy of numerical models starts from the heave and pitch motions. For the RAOs of these oscillatory motions, a fair to good agreement between the experimental values and the numerical results is in general assessed. In more detail, the pitch motion in head waves (Figure 2) is predicted well, apart from a slight overestimation by the numerical models of the second resonant peak around an L_{PP}/λ_W ratio of 2.3. This behaviour can be ascribed, among other possibilities, to the insufficient damping due to the neglected viscous effects in potential codes, as suggested in [12] and discussed in the introduction. In following waves (Figure 3), the comparison of pitch RAOs looks worse, with relevant overestimations by the numerical codes at the three higher speeds. The overestimation worsens with the decrease of the wave length. This is supposedly related to phenomenon described in the previous section: at moderate forward speeds, following waves are slowed down by the return current and therefore their influence does not extend to the full length of the ship, reducing the oscillatory motions in the experimental results. For the cases where the return current is fast enough to stop the wave propagation with respect to the ship's speed, e.g. for the last wave length at Fr = 0.100 and the last two at Fr = 0.125, the experimental values of the pitch RAO are close to zero, further confirming the hypothesis that in such cases the incoming waves cannot reach the ship. For heave motion, analogous considerations can be drawn. Concerning the difference between the strip theory code Seaway and the 3D panel code Hydrostar, in head waves the two codes compare quite similarly, with Hydrostar showing a slightly better agreement with experiments. In following waves, the results of Seaway are clearly contaminated by a shift of the results towards shorter wave lengths with respect to the results of Hydrostar. This Seaway result is theoretically wrong, it increases with the ship speed and is not present in head waves. Therefore, it is attributed to a bug in the implementation of the dispersion relation in following waves with forward speed in the Seaway code. The phases of the heave and pitch motions are not shown in this paper for reasons of space, but a satisfactory agreement between the numerical results and the experiments is assessed apart from a few discordant cases.

Concerning the added resistance, the results are shown in Figure 6 and Figure 7. Since the results of Hydrostar consistently outperform the results of Seaway, the following analysis will focus only on results of the 3D panel code. In head waves, the results of the 3D code correctly describe the asymptotic short-wave trend of added resistance shown by the experiments. However, in the long waves range the agreement with the experiments is much worse, with the numerical results following different patterns. Apparently, the numerical model is not capable of accurately describing the added resistance in shallow water with forward speed. However, it is not clear whether the responsibility of this lies in the algorithm for the calculation of the added resistance (near-field method) or in the discrepancies already noticed in the simulated vertical motions, which are expected to heavily influence the added resistance as described in the introduction. According to Pinkster [8], the dominant term in the near-field formulation for added resistance can be expressed as an integral over the waterline of the relative wave elevation squared:

$$-0.5 \cdot \rho g \int_{WL} \zeta_{\mathrm{rel}}^2 n_1 dl \tag{3}$$

In order to calculate the added resistance induced by the dominant term expressed by Equation (3), the waterline of the vessel at the selected draft is discretised in 20 linear segments of different lengths. For each segment, the length, x coordinate of the midpoint and normal direction are derived. Then, the relative wave elevation at segment midpoints is calculated based on the x coordinate of the midpoint and on amplitudes and phases of the incident regular wave and of the heave and pitch motions. As an approximation, only the wave elevation induced by the incident wave is considered in the calculation of the relative wave elevation, neglecting the effects of radiated and diffracted waves. Finally, the integral of Equation (3) is solved in a discrete way by summing up the terms corresponding to each linear segment. The results, compared with the total added resistance, are shown in Figure 9 for three ship speeds and for both the 3D code and experimental results. Similar results are obtained for the other speeds as well.

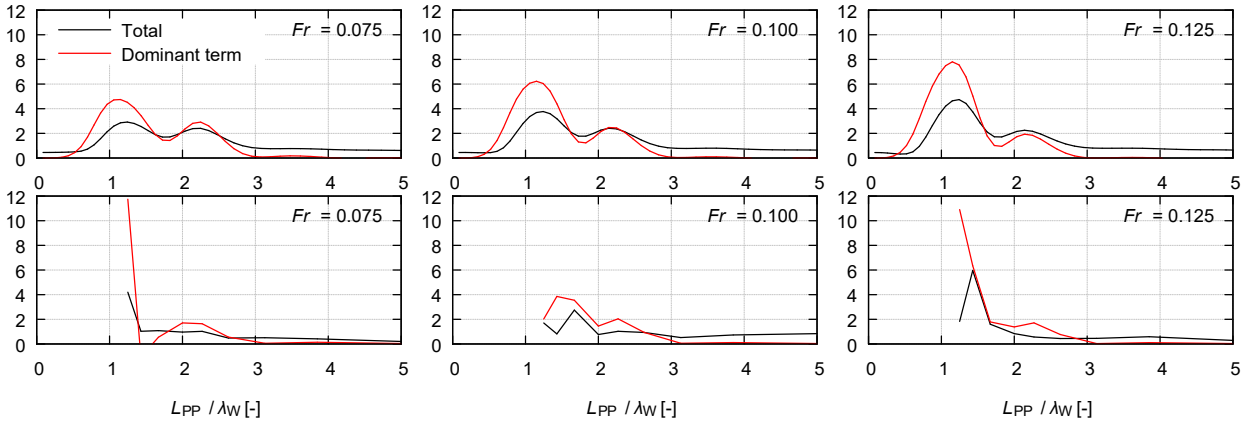

Figure 9: Comparison of total added resitance and dominant term calculated according to Equation (3) for BEM code results (top plots) and experiments with Frame A and ζ_A = 11.1 mm (bottom plots).

Figure 9 shows that, even in the shallow water conditions under investigation, the term dependent on relative wave elevation along the waterline has a dominant role: the pattern outlined by this term closely matches the one shown by the total added resistance in both the numerical and experimental results. The total added resistance has a lower magnitude than the dominant term due to the expected reductions induced by the other, less influential terms [11]. Since the dominant term is tightly related to the vertical motions, the matching patterns outlined in Figure 9 prove that the inaccuracies in the simulated added resistance are to be ascribed mainly to the inaccurately simulated motions of heave and pitch.

In following waves, the numerical model seems to capture at least the trend outlined by experiments except for the parts where the peculiar physical phenomenon described in the previous section occurs. This phenomenon cannot be simulated with presently available potential codes and will need to be further investigated in future research with more advanced tools.

5 CONCLUSION

The paper focuses on added wave resistance in shallow water, a topic seldom analysed in literature. The added resistance of an Ultra Large Container Ship (ULCS) with a non-dimensional UKC of 50% is investigated through model tests and simulations with potential flow codes, for both head and following regular waves.

The experimental results first of all show that the added resistance is proportional to the square of the wave amplitude. Secondly, two main ranges of wave lengths are identified in which the added resistance shows a distinct behaviour. In the long waves range, corresponding approximately to waves longer than one third of L_{PP}, the added resistance is shown to be strictly related to the vertical oscillatory motions of heave and pitch. In the short waves range, on the other hand, an asymptotic behaviour of the added resistance is observed. These two behaviours are similar to what is generally observed in deep water conditions.

In following waves, a peculiar phenomenon is noticed and, according to the author's best knowledge, described in detail for the first time in literature. At moderate forward speeds a positive added resistance is

measured for a specific, speed dependent interval of wave lengths. The magnitude of this added resistance is large, even higher than the one associated with head waves. The reason for this is preliminary ascribed to the interaction between the return current generated by the forward motion of the ship in shallow water and the incident wave field.

Simple calculations are presented based on the group velocity of incident waves and on the mean return flow generated by the ship. These calculations show that the positive added resistance in following waves occur when the group velocity of waves relative to the moving ship is low. This results in a peculiar flow condition where the front of the wave disturbance is located along the ship's length for a significant part of the test. The positive added resistance in following waves is deemed as a very interesting phenomenon, to be further investigated in future research.

Numerical simulations are performed with a strip theory code and with a 3D panel code, and the results are compared with experiments. The 3D panel code is shown to perform better than the strip theory code. In head waves, the added resistance simulated by potential codes does not match the experimentally measured one. An analysis on the influence of vertical motions on the added resistance is performed, showing that the inaccuracies in the simulation of added resistance can be mainly ascribed to the inaccurately simulated RAOs and phases of vertical motions. In following waves, discrepancies between the experimental and numerical results are mainly due to the positive added resistance induced by the return flow, which cannot be modelled by presently available potential flow solvers.

ACKNOWLEDGEMENTS

The present work is performed in the frame of project WL_2017_06 (Scientific support for the implementation of seakeeping in the ship manoeuvring simulators), while the experimental campaign was performed in the frame of project WL_2013_47 (Scientific support for investigating the manoeuvring behaviour of ships in waves). Both projects are granted to Ghent University by Flanders Hydraulics Research, Antwerp (Department of Mobility and Public Works, Flemish Government, Belgium).

For the numerical calculations a research Hydrostar licence was provided by Bureau Veritas through their Antwerp and Paris offices, which is highly appreciated.

REFERENCES

[1] Maruo, H. "The drift of a body floating in waves". In: *Journal of Ship Research* 4.3 (1960), pp. 1–10.

[2] Joosen, W. P. A. "Added resistance of ships in waves", In: *Proceedings of the 6th Symposium on Naval Hydrodynamics*, Washington D.C., USA, 1966.

[3] Newman, J. N. "The drift force and moment on ships in waves". In: *Journal of Ship Research* 11.1 (1967), pp. 51–60.

[4] Gerritsma, J. and W. Beukelman. "Analysis of the resistance increase in waves of a fast cargo ship". In: *International Shipbuilding Progress* 19.217 (1972), pp. 285–293.

[5] Liu, S., A. Papanikolaou, and G. Zaraphonitis. "Prediction of added resistance of ships in waves". In: *Ocean Engineering* 38.4 (2011), pp. 641–650.

[6] Havelock, T. H. "The resistance of a ship among waves". In: *Proceedings of the Royal Society of London A* 161.906 (1937), pp. 299–308.

[7] Boese, P. "Eine einfache Methode zur Berechnung der Widerstandserhöhung eines Schiffes im Seegang". In: *Journal Schiffstechnik - Ship Technology Research* 17.86 (1970).

[8] Pinkster, J. A. "Mean and low frequency wave drifting forces on floating structures". In: *Ocean Engineering* 6.6 (1979), pp. 593–615.

[9] Faltinsen, O. M., K. J. Minsaas, N. Liapis, and S. O. Skjørdal. "Prediction of Resistance and Propulsion of a Ship in a Seaway", In: *Proceedings of the 13th Symposium on Naval Hydrodynamics*, Tokyo, Japan, 1980, pp. 505–529.

[10] Seo, M. G., D. M. Park, K. K. Yang, and Y. Kim. "Comparative study on computation of ship added resistance in waves". In: *Ocean Engineering* 73 (2013), pp. 1–15.

[11] Pinkster, J. A. "Low frequency second order wave exciting forces on floating Structures". PhD thesis. Technical University of Delft, 1980.

[12] Kim, M., O. Hizir, O. Turan, S. Day, and A. Incecik. "Estimation of added resistance and ship speed loss in a seaway". In: *Ocean Engineering* 141 (2017), pp. 465–476.

[13] Yu, J.-W., C.-M. Lee, J.-E. Choi, and I. Lee. "Effect of ship motions on added resistance in regular head waves of KVLCC2". In: *Ocean Engineering* 146 (2017), pp. 375–387.

[14] Sigmund, S. and O. el Moctar. “Numerical and experimental investigation of added resistance of different ship types in short and long waves”. In: *Ocean Engineering* 147 (2018), pp. 51–67.
[15] Fujii, H. and T. Takahashi. “Experimental study on the resistance increase of a ship in regular oblique waves”, In: *Proceedings of the 14th ITTC, Vol. 4*, 1975, pp. 351–360.
[16] Liu, S., A. Papanikolaou, and G. Zaraphonitis. “Practical approach to the Added Resistance of a Ship in Short Waves”, In: *Proceedings of the 25th International Ocean and Polar Engineering Conference (ISOPE)*, Kona, Big Island, Hawaii (USA), 2015, pp. 11–18.
[17] Yang, K.-K., Y. Kim, and Y.-W. Jung. “Enhancement of asymptotic formula for added resistance of ships in short waves”. In: *Ocean Engineering* 148 (2018), pp. 211–222.
[18] Kim, M., O. Hizir, O. Turan, and A. Incecik. “Numerical studies on added resistance and motions of KVLCC2 in head seas for various ship speeds”. In: *Ocean Engineering* 140 (2017), pp. 466–476.
[19] Chen, S., T. Hino, N. Ma, and X. Gu. “RANS investigation of influence of wave steepness on ship motions and added resistance in regular waves”. In: *Journal of Marine Science and Technology* 23 (2018), pp. 991–1003.
[20] Tello Ruiz, M., S. De Caluwé, T. Van Zwijnsvooorde, G. Delefortrie, and M. Vantorre. “Wave effects in 6DOF on a ship in shallow water”, In: *Proceedings of MARSIM 2015*, Newcastle, UK, 2015, pp. 1–15.
[21] Tello Ruiz, M., G. Delefortrie, and M. Vantorre. “Induced wave forces on a ship manoeuvring in coastal waves”. In: *Ocean Engineering* 121 (2016), pp. 472–491.
[22] Tello Ruiz, M., M. Mansuy, G. Delefortrie, and M. Vantorre. “Modelling the manoeuvring behaviour of an ULCS in coastal waves”. In: *Ocean Engineering* 172 (2019), pp. 213–233.
[23] Martić, I., G. Chillcce, M. Tello Ruiz, J. Ramirez, N. Degiuli, and B. O. el Moctar. “Numerical assessment of added resistance in waves of the DTC container ship in finite water depth”, In: *Proceedings of the 5th International Conference on Ship Manoeuvring in Shallow and Confined Water (MASHCON)*, Ostend, Belgium, 2019, pp. 274–283.
[24] Van Zwijnsvooorde, T., M. Tello Ruiz, G. Delefortrie, and E. Lataire. “Sailing in Shallow Water Waves with the DTC Container Carrier: Open Model Test Data for Validation Purposes”, In: *Proceedings of the 5th International Conference on Ship Manoeuvring in Shallow and Confined Water (MASHCON)*, Ostend, Belgium, 2019, pp. 412–421.
[25] Delefortrie, G., S. Geerts, and M. Vantorre. “The towing tank for manoeuvres in shallow water”, In: *Proceedings of the 4th International Conference on Ship Manoeuvring in Shallow and Confined Water (MASHCON)*, Hamburg, Germany, 2016, pp. 226–235.
[26] Tello Ruiz, M., M. Vantorre, T. Van Zwijnsvoorde, and G. Delefortrie. “Challenges with ship model tests in shallow water.”, In: *Proceedings of the 12th International Conference on Hydrodynamics (ICHD)*, Egmond aan Zee, The Netherlands, 2016, pp. 59, 1–10.
[27] Mansuy, M., M. Tello Ruiz, G. Delefortrie, and M. Vantorre. “Post processing techniques study for seakeeping tests in shallow water”, In: *AMT 2017*, Glasgow, UK, 2017, pp. 460–473.
[28] Journée, J. M. . and L. M. J. Adegeest. “Theoretical Manual of Strip Theory Program “SEAWAY for Windows”. Report 1370”, (2003).
[29] Vantorre, M. and J. Journée. “Validation of the strip theory code SEAWAY by model tests in very shallow water”, Antwerp, Belgium, (2003).
[30] Gourlay, T., E. Lataire, G. Delefortrie, L. Donatini, M. Tello Ruiz, D. Veen, T. Bunnik, and R. P. Dallinga. “Benchmarking of DIFFRAC, FATIMA, HydroSTAR, MOSES, NEMOH, OCTOPUS, PDStrip, RAPID, SEAWAY, SlenderFlow and WAMIT against measured vertical motions of the Duisburg Test Case container ship in shallow water.”, In: *Proceedings of the 5th MASHCON conference*, Ostend, Belgium, 2019, pp. 156–163.
[31] Svendsen, I. A. *Introduction to Nearshore Hydrodynamics*. World Scientific Publishing Co. Pte Ltd, 2005.
[32] Newman, J. N. *Marine hydrodynamics*. Massachusetts: MIT Press, 1977.